

Article

# Improving the RST-OIL Algorithm for Oil Spill Detection under Severe Sun Glint Conditions

Valeria Satriano <sup>1</sup>, Emanuele Ciancia <sup>1</sup>, Teodosio Lacava <sup>2,\*</sup>, Nicola Pergola <sup>2</sup> and Valerio Tramutoli <sup>1</sup>

<sup>1</sup> School of Engineering, University of Basilicata, Via dell'Ateneo Lucano 10, 85100 Potenza, Italy; valeria.satriano@unibas.it (V.S.); emanuele.ciancia@imaa.cnr.it (E.C.); valerio.tramutoli@unibas.it (V.T.)

<sup>2</sup> Institute of Methodologies for Environmental Analysis (IMAA), CNR, C.da S. Loja, 85050 Tito Scalo, Italy; nicola.pergola@imaa.cnr.it

\* Correspondence: teodosio.lacava@imaa.cnr.it; Tel.: +39-0971-427242

Received: 29 May 2019; Accepted: 21 November 2019; Published: 23 November 2019



**Abstract:** In recent years, the risk related to oil spill accidents has significantly increased due to a global growth in offshore extraction and oil maritime transport. To ensure sea safety, the implementation of a monitoring system able to provide real-time coverage of large areas and a timely alarm in case of accidents is of major importance. Satellite remote sensing, thanks to its inherent peculiarities, has become an essential component in such a system. Recently, the general Robust Satellite Technique (RST) approach has been successfully applied to oil spill detection (RST-OIL) using optical band satellite data. In this paper, an advanced configuration of RST-OIL is presented, and we aim to extend its applicability to a larger set of observation conditions, referring, in particular, to those in the presence of severe sun glint effects that generate some detection limits to the RST-OIL standard algorithm. To test such a configuration, the DeepWater Horizon platform accident from April 2010 was selected as a test case. We analyzed a time series of Moderate Resolution Imaging Spectroradiometer (MODIS) images that are usually significantly affected by sun glint in the Gulf of Mexico area. The accuracy of the achieved results was evaluated for comparison with a well-established satellite methodology based on microwave data, which confirms the potential of the proposed approach in identifying the oil presence on the scene with good accuracy and reliability, even in these severe conditions.

**Keywords:** oil spill; MODIS; optical band; near infrared; sun glint; DeepWater Horizon; RST-OIL

## 1. Introduction

Among the different pollution sources that may affect marine ecosystems, oil spills are one of the most dangerous from an environmental point of view, especially when they involve a coastal habitat. Oil contamination can affect the sea environment in different ways, such as by natural leakages (crude oil coming from sedimentary rocks), discharges resulting from routine operations on ships, and due to large accidents involving tankers and/or oil extraction platforms [1]. Apart from a few situations where natural oil seeps may even support benthic ecosystems [2], oil spills can cause irreversible damage to marine ecosystems, not only in terms of seawater and coastal zone pollution, but also regarding the health of the flora and fauna living in the area.

Considering only spills related to anthropic activity, in the last few decades, the number of large spills (>700 tons) related to tanker accidents, as well as the number of medium-sized ones (7–700 tons), have decreased significantly [3]. Despite such a reduction, large spills are still able to affect, in terms of volume, the total amount of oil dispersed annually in the sea [3]. Even in the case of such accidents, the success of the actions aimed at reducing the environmental after-effects is strictly linked to the timeliness of the identification and the accuracy in predicting the displacement (and/or dispersion) [4].

In this framework, the development of efficient monitoring systems able to provide timely information about the seawater status is essential.

Remote sensing has become an integral part of modern response systems [5] to oil spill accidents, and several techniques based on different data have been developed to address this aim. Synthetic Aperture Radars (SAR) are the most widely used satellite systems for marine pollution control, due to their capability to identify oil spills with good sensitivity and a high spatial resolution (up to 1 m) [5–12]. SAR systems allow for almost all-day and all-weather detection that is not dependent on the presence of a natural source of electromagnetic radiation and is not affected by the cloud presence. However, their operational use in a continuous monitoring procedure is mainly limited to their low repetition time (from a few days to dozens of days, at mid latitudes and for a single satellite), specific wind range speed conditions, and a possible look-alike presence [5–12]. Cosmo-SkyMed [13] and the recent Sentinel-1 Copernicus missions, both working in a satellite constellation configuration, allowed the issues to be reduced due to the low repetition time, which allows for more frequent temporal sampling (from 12 h up to 5–6 days).

In this context, passive optical sensors, on-board meteorological satellites, and constellations of low Earth orbiting polar satellites could represent a good alternative. Even if with lower spatial resolutions (from 250 m up to 3 km) than SAR systems, optical sensors guarantee a higher temporal resolution (up to a few hours for polar satellites and a few minutes for geostationary ones), which is more useful for real-time monitoring of areas affected by oil pollution risk. Their usability is, however, influenced by cloud cover, in which the presence may hamper any sea surface acquisition.

Up until now, techniques developed for oil spill detection in the optical region have generally exploited a particular observational geometry and have used the difference between measured signals (e.g., brightness temperature or spectral reflectance) over the oil-affected areas and the neighboring clean sea surface. However, the use of fixed thresholds sometimes makes it difficult to discriminate between oil-originated signals and normal sea surface fluctuations when different environmental and observational conditions are considered [5,14–24]. Furthermore, they are also primarily designed to provide detailed mapping of the affected areas only once oil presence is known, which results in them not being particularly useful for providing the first alert. The suitable spectral region for oil recognition ranges from the visible (VIS)-near infrared (NIR), namely the VNIR region, to the thermal infrared (TIR). In the TIR region, oil is discriminated against surrounding water due to the different brightness temperatures of the two elements directly related to their own thermal inertia characteristics and the oil type and thickness [5,14,25–30]. In the VNIR, discrimination is based on the different oil and water reflectance properties. However, this difference is not unique and it is possible that the oil presence on the sea surface produces both an increase (positive contrast) and a decrease (negative contrast) in reflectance due to the different unpredictable factors related to the acquisition geometry (zenith and azimuth sun-sensors angles) as well as oil and environmental characteristics [31–34].

Among the optical methods, the Robust Satellite Technique (RST) [35] specifically applied to oil spill detection, namely RST-OIL [27,28,36–38], has been demonstrated to detect the oil presence, using both TIR (in terms of brightness temperature) and VNIR (in terms of Rayleigh-corrected reflectance) data using automatic, self-adaptive thresholds. The methodology identifies significant statistical deviation of the measured signal on the basis of its preliminary characterization in terms of the expected value (temporal mean) and normal variability (standard deviation). To this aim, historical long-term time series of satellite data that are homogeneous in the spectral, spatial, and temporal domains are analyzed.

In this work, an advanced RST-OIL configuration is proposed, especially for data acquired in the NIR band (i.e.,  $0.8 \mu\text{m}$ ) by the Moderate Resolution Spectroradiometer (MODIS) with the main goal being to face some limits appearing when the sun glint affects the investigated scene. For a differential approach like RST, the random appearance of glint/no-glint conditions may have a negative impact on the characterization of the expected signal (i.e., on the temporal mean and standard deviation computation). Thus, the proposed new RST-OIL configuration aims to extend its application to different observation conditions in order to further enlarge its range of applicability. The spill event caused by the explosion and sinking of the DeepWater Horizon Platform (DWH) in the Gulf of Mexico has been selected as a test case. The accident started on 20 April 2010 and continued up until 15 July 2010, and produced a total of about 5 million barrels of spilled oil. This event prompted scientists, the academic community, and the private sector to spend their work and time finding modern technologies to map the spilled oil and simulate its transport over the sea in order to give a rapid response and manage the effects on the environment [39]. One of the peculiarities of the area is that, at the time of Aqua and Terra satellites overpass (i.e., the two satellites carrying MODIS onboard), it can exhibit different sun-satellite geometry acquisitions up to severe sun glint conditions, which represents a suitable case study for testing the new proposed RST-OIL configuration.

## 2. Materials and Methods

### 2.1. Data

MODIS Level 1B (L1B) and the corresponding Geolocation (GEO) data acquired by Terra and Aqua satellites were used in this work. Such L1B data, downloaded from the NASA-LAADS DAAC (National Aeronautics and Space Administration-Level-1 and Atmosphere Archive and Distribution System Distributed Active Archive Center) website [40], were processed over the Gulf of Mexico for the months of April and May within the 2003–2010 time interval. In detail, 348 and 472 images were collected for April and May respectively, producing four different datasets, one for each month and satellite considered. Then, a spectral/spatial sub-setting was carried out by means of HDFLook software (developed under collaboration between the Laboratoire d'Optique Atmosphérique and the Goddard Earth Sciences Distributed Active Archive Center), which was aimed at producing historical series of  $0.8$  and  $12 \mu\text{m}$  (TIR) band signals for a sub-set centered on the DeepWater Horizon Platform (DWH) platform location (i.e.,  $28.74$  Lat N,  $88.39$  Lon W), and re-projected in Lat/Lon WGS-84 (Figure 1). The above-mentioned sub-set (at a  $1\text{-km}$  spatial resolution) was also produced starting from the GEO (i.e., geolocation) file to create the same output for the sensor and solar azimuth and zenith angles. NIR data were used at a full spatial resolution (i.e.,  $250\text{ m}$ ) to implement the methodology proposed in this paper, while TIR data (at a  $1\text{-km}$  spatial resolution) allowed for cloud screening, which will be discussed later. The azimuth and zenith angles were exploited for identifying sun glint conditions.

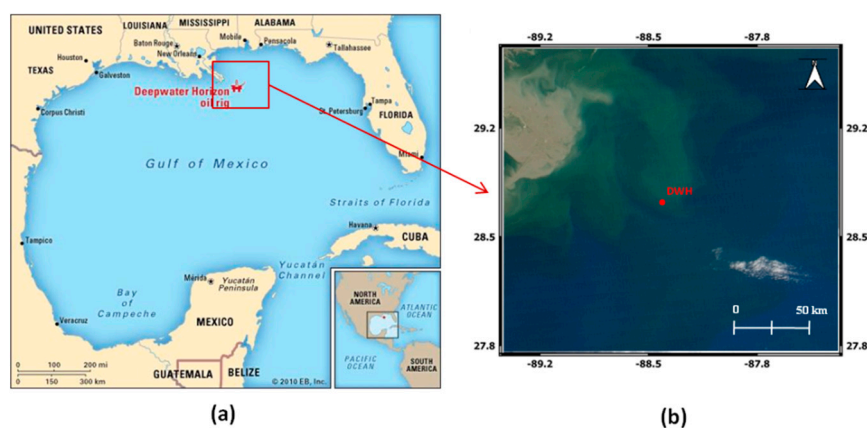


**Figure 1.** (a) DeepWater Horizon Platform (DWH) localization in the Gulf of Mexico. (b) True color Red Green Blue (RGB) of the Region of Interest (ROI) used in this work.

## 2.2. RST-OIL

The RST approach is an automatic change-detection scheme based on the analysis of historical series of satellite data for complete signal characterization (spectral, spatial, and temporal) followed by an anomaly detection step implemented by using automatically generated local (i.e., for a specific time and place of observation) self-adaptive thresholds. A full description of the methodology can be found in Reference [35]. In its previous configuration, devoted to the automatic and timely detection of oil spills, namely RST-OIL, it was implemented on Advanced Very High Resolution Radiometer (AVHRR) and MODIS TIR data [27,28,36,37], which demonstrates good performance regardless of the observation and environmental conditions. This enabled the detection of different oil spills that occurred in several areas worldwide. RST-OIL has been recently successfully tested in the VIS and NIR MODIS channels, using the corresponding Rayleigh-corrected reflectance ( $R_{rc}$ ) data to detect an illicit vessel discharge that occurred off the south coast of Cyprus in June 2007 [38].

As mentioned above, the new configuration proposed in this work is based on MODIS NIR data. Therefore, the Absolutely Local Index of Change of the Environment (ALICE) was implemented as follows.

$$\otimes_{R_\lambda}(x, y, t) = \frac{[R_\lambda(x, y, t) - \mu_{R_\lambda}(x, y)]}{\sigma_{R_\lambda}(x, y)} \quad (1)$$

where  $R_\lambda(x, y, t)$  is the MODIS reflectance at  $\lambda = 0.8 \mu\text{m}$ .  $\mu_{R_\lambda}(x, y)$  and  $\sigma_{R_\lambda}(x, y)$  are the temporal mean and standard deviation signals, respectively (namely reference fields) computed by analyzing a long-term dataset of homogeneous satellite records collected at the pixel location  $x, y$  under the same observation conditions (the same month of the year and the same time of acquisition) of the image under investigation. To make the reference fields actually representative of unperturbed conditions, for each pixel  $(x, y)$  of the study area, an iterative  $k\sigma$ -clipping procedure [35] was implemented to exclude possible outliers [41]. The ALICE index is a standardized variable that can be described through a normal (or Gaussian) distribution with zero mean ( $\mu$ ) and variance ( $\sigma$ ) equal to 1. Therefore, the probability of occurrence of values above  $2\sigma$  (i.e.,  $R_\lambda > \mu_{R_\lambda} + 2\sigma_{R_\lambda}$ ) or below  $-2\sigma$  (i.e.,  $R_\lambda < \mu_{R_\lambda} - 2\sigma_{R_\lambda}$ ) is about 2.5% and falls to 0.15% for values above  $3\sigma$  (or below  $-3\sigma$ ). Taking into account the above-described dual behavior of oil in the NIR band, the corresponding index  $\otimes_{R_{0.8}}$  would show high and positive values (at least  $\otimes_{R_{0.8}} > 2$ ) for pixels characterized by a positive oil/seawater contrast and the opposite behavior (at least  $\otimes_{R_{0.8}} < 0$ ) in case of a negative contrast. The latter, where the reflectance is limited to positive values, which are very low in the NIR band for unperturbed conditions, is an expected behavior that may, in some cases, result in sensitivity issues or missing detections (i.e., false negatives).

In order to avoid false alarms related to the high NIR signals of clouds, the latter have been previously identified and discarded from the ALICE computation. Clouds were recognized by using the One-channel Cloudy-Radiance detection Approach (OCA) [42]. The standard OCA approach involves the combined use of TIR and VIS information to identify unexpected low temperatures or high reflective pixels related to the cloud presence. Unfortunately, in the VIS region, clouds and oil often exhibit similar spectral behavior, and, therefore, it was not possible to use the VIS band here. Hence, the TIR signal was exploited as a unique input to generate a binary cloud mask. Since TIR data are at 1 km of spatial resolution, a downscaling procedure has been implemented by a C++ code developed ad hoc and applied to the cloud mask to co-locate it on the corresponding NIR imagery at a spatial resolution of 250 m.

### 2.3. Extending the Applicability of RST-OIL to Different Observational Conditions

A differential multi-temporal approach like RST-OIL may suffer in terms of reliability when the unperturbed conditions, represented by the temporal mean, show a large variability in the investigated temporal dataset. The previously mentioned  $k\sigma$ -clipping procedure [35,41], implemented during the reference field computation, aims to eliminate outlier values from the historical dataset, which are those values that are well above (or below) the “normal” range identified by the  $\mu \pm k\sigma$  interval. For example, in an area where sun glint is randomly present, the reflectance rise on the sea surface (usually very high) in such conditions is automatically eliminated by this procedure. Therefore, the computed reference fields are not perturbed by this contribution, which results in a more representative expected signal and variability in the absence of sun glint. Hence, during the ALICE (Equation (1)) computation, the presence of sun glint in the image under investigation will produce high positive values regardless of the presence of oil.

In order to better understand the high reflectance variation when the glint effect appears on the scene, in Figure 2, an example of the study area in glint (Figure 2a) and no glint (Figure 2b) conditions is given. In both images, the top panel represents the scene in a natural Red Green Blue (RGB) color code, while the bottom one refers to the NIR acquisition. In the latter, the signals arising from clouds and land and coastal zones (masked in purple) were not considered to focus better on the clear seawater contribution. Focusing on the NIR images, the sea surface reflectance variability under no glint conditions (Figure 2a) shows an expected pattern, with low values ranging in a very small interval (1–2%) typical of the sea surface in this spectral range. When sun glint affects the scene (Figure 2b), the values increase by up to 10% as does their spatial variability range (9%). Such a random increase may represent an outlier within the whole temporal dataset and, hence, may be discarded during the  $k\sigma$ -clipping procedure.

In order to overcome this possible issue and make the approach as exportable as possible, the signal variations due to different sun-satellite geometries within the reference fields’ computation process should be taken into account. To this aim, a general criterion based only on satellite data was implemented. The choice for avoiding the use of any kind of ancillary information (i.e., wind speed [43]), which might not be always available at the requested spatiotemporal scale, is related to the need to develop a general criterion that can be easily implemented. In detail, for each of the pieces of L1B data within the considered datasets, starting from sensor and solar zenith ( $\phi_s$  and  $\phi_0$ , respectively) and azimuth angles ( $\omega_s$  and  $\omega_0$ , respectively), each pixel ( $x,y$ ) was flagged as a glint (G), high glint (HG), or no glint (NG) pixel, computing the glint angle ( $\theta_g$ ) as follows [23].

$$\theta_g = \arccos (\cos \varphi_s \cos \varphi_0 + \sin \varphi_s \sin \varphi_0 \cos \Delta\omega) \quad (2)$$

where  $\Delta\omega$  is the difference between the satellite-solar azimuth angles. If  $\theta_g < 40^\circ$ , the relative pixel is in high glint. If the value ranges between  $40^\circ$  and  $60^\circ$ , it is in glint. Otherwise, for  $\theta_g > 60^\circ$ , it is not in a glint condition. The threshold values were derived from the analysis of the  $\theta_g$  variation on the entire available dataset.

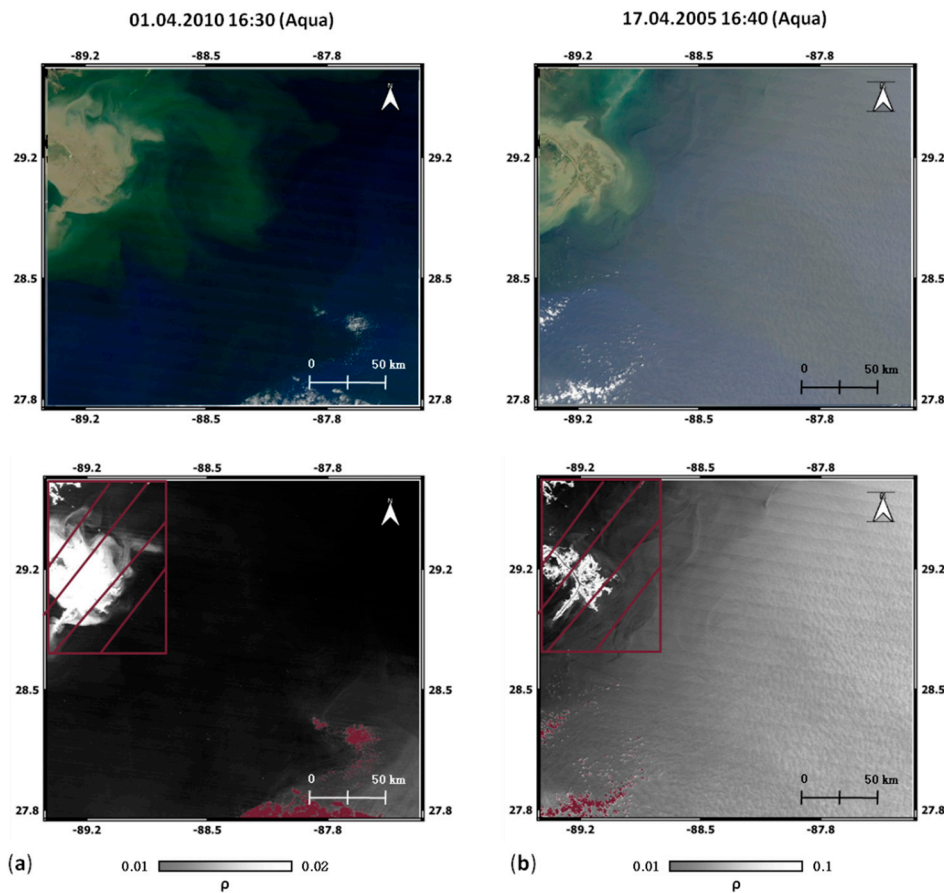


**Figure 2.** An example of the study area under no glint (a) and glint (b) conditions: RGB (top) and NIR-0.8  $\mu\text{m}$  (bottom) image. Purple areas were not considered in the analysis.

Therefore, after the application of the previously mentioned criterion (Equation (2)), the whole dataset was further divided, at a pixel level, into homogeneous (i.e., glint, high glint, or no glint) classes (Figure 3) to produce the corresponding reference fields, for glint (i.e.,  $\mu_{R_\lambda, G}(x, y, \theta_g)$  and  $\sigma_{R_\lambda, G}(x, y, \theta_g)$ ), high glint (i.e.,  $\mu_{R_\lambda, HG}(x, y, \theta_g)$  and  $\sigma_{R_\lambda, HG}(x, y, \theta_g)$ ), and no glint (i.e.,  $\mu_{R_\lambda, NG}(x, y, \theta_g)$  and  $\sigma_{R_\lambda, NG}(x, y, \theta_g)$ ) conditions, respectively. Equation (1) results were then modified as follows (hereafter called  $\text{ALICE}_{R^*\lambda}$ ).

$$\otimes_{R^*\lambda}(x, y, t, \theta_g) = \frac{[R_\lambda(x, y, t, \theta_g) - \mu_{R_\lambda}(x, y, \theta_g)]}{\sigma_{R_\lambda}(x, y, \theta_g)} \quad (3)$$

These reference fields will allow for better characterization of the measured signal in more homogenous environmental conditions. For a historical data set of images acquired under glint (or high glint) conditions, the computed mean value will be high, and, hence, during ALICE (Equation (3)) computation, the relative comparison with an image acquired under the same observation conditions should not produce high values of the indicator, except in the presence of other perturbing factors (e.g., oil on the scene).

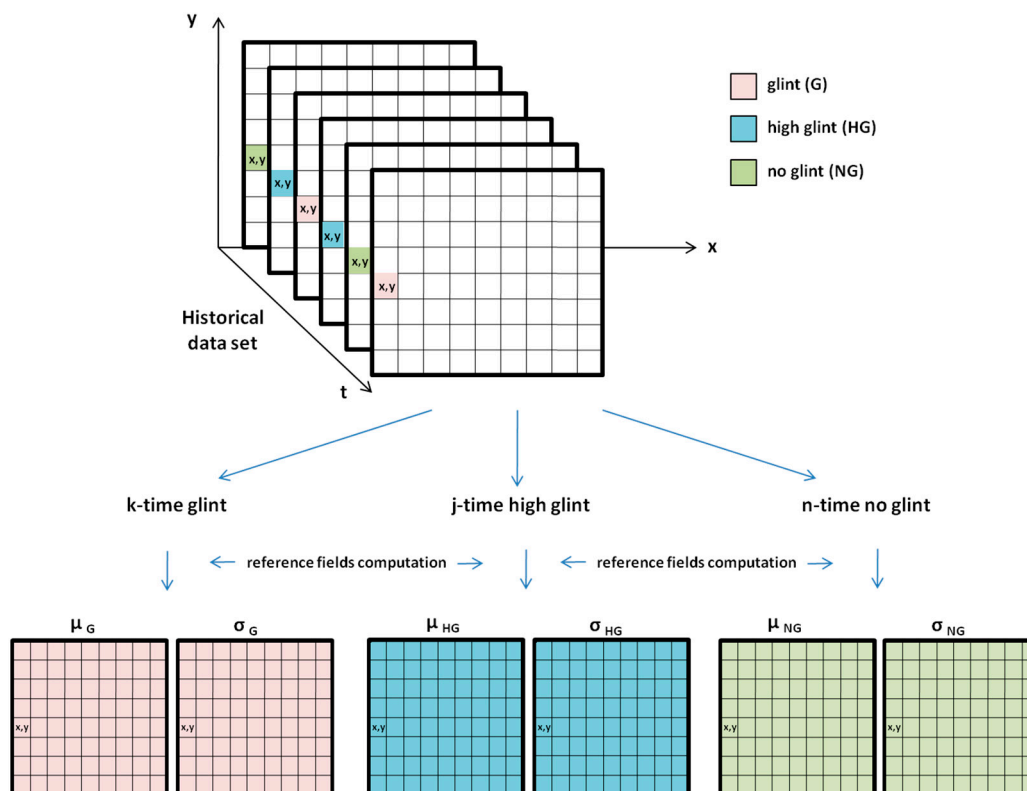


Figure 3. Logical flux for reference field computation.

According to Equation (3), the  $\otimes_{R^{*0.8}}$  index has been computed at the pixel level for homogeneous classes depending on the occurrence of the previously recognized conditions with a particular focus on glint and high glint ones.

### 3. Results

The potential of the proposed approach for detecting oil spills under severe observation conditions with a good trade-off between reliability and sensitivity has been tested by analyzing images acquired during the DWH accident (April–May 2010), where the oil presence has already been detected by other methodologies [5,22,23,44–46]. It should be stressed that almost all the images are affected by sun glint. Hence, in the following section, we mostly focus on these specific conditions. Images were first investigated by implementing the standard RST-OIL configuration (i.e., using the reference fields computed as described in Section 3.1) and then the one specifically proposed in this paper (Section 3.2).

#### 3.1. Standard RST-OIL Results

The first available no-cloudy Aqua image related to the DWH area is the one from 25 April 2010 at 18:55 GMT (LT = GMT-6) (Figure 4a), while, for the Terra satellite, the first useful image is from 29 April 2010 at 16.55 GMT (Figure 4b). These two images have been used to test the difference between the results achievable with the RST-OIL standard configuration and the advanced one proposed in this work. Figure 4a,b show average  $\theta_g$  values lower than  $40^\circ$  ( $31^\circ$  and  $34^\circ$ , respectively) indicating a contribution to the total signal coming from the high glint effect (Section 2.3). In both images, the area affected by the oil spill (i.e., the bright spatial feature around the DWH location), shows a positive contrast against the surrounding seawater.

In order to quantitatively assess such a contrast, the  $R_{0.8}$  signal variability along the transect Z-Z' was investigated (Figure 5), and the relative reflectance trend is shown in Figure 5b, where it is possible to note the clear increase (up to 100% of variation) in correspondence of the oil affected area. A very similar behavior was found for the Terra image (Figure 6). In both cases, the  $R_{0.8}$  measured for the

clear sea surface was also relatively high (over 6%), which confirmed that a possible contribution from the atmosphere and/or a relation with acquisition geometry has to be taken into account. To this aim, an analysis carried out on  $R_{rc}$  values in the same NIR spectral band (not shown here) for the Aqua and Terra images (Figure 4), indicated that, even after removing the aerosol contribution, the sea surface signal still showed high values in both images, which confirmed the impact of sun glint on these acquisitions.

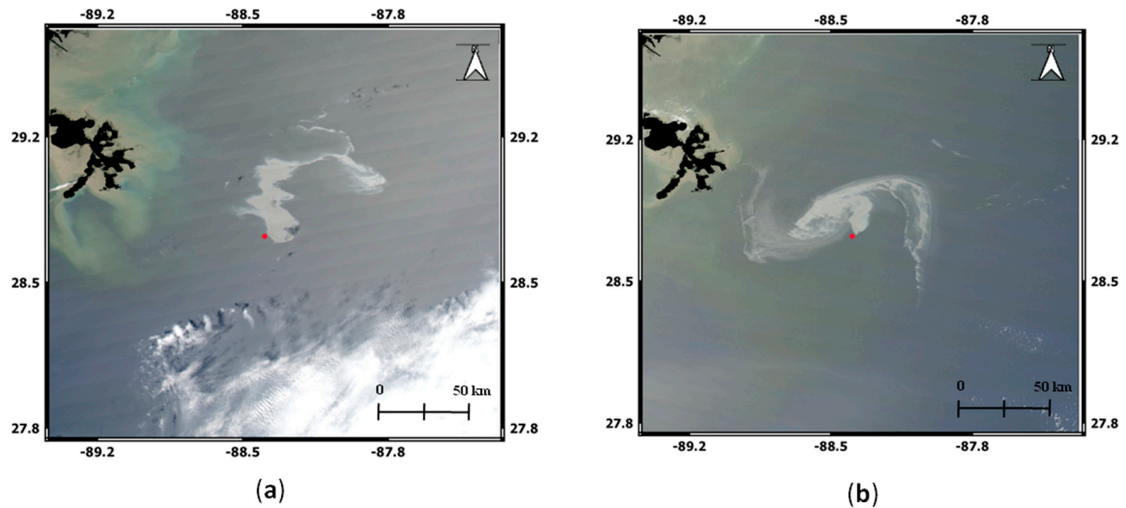


**Figure 4.** (a) MODIS-Aqua true color RGB image from 25 April 2010 at 18:55 GMT, (b) MODIS-Terra true color RGB image from 29 April 2010 at 16:55 GMT. The red star indicates the DWH platform position.

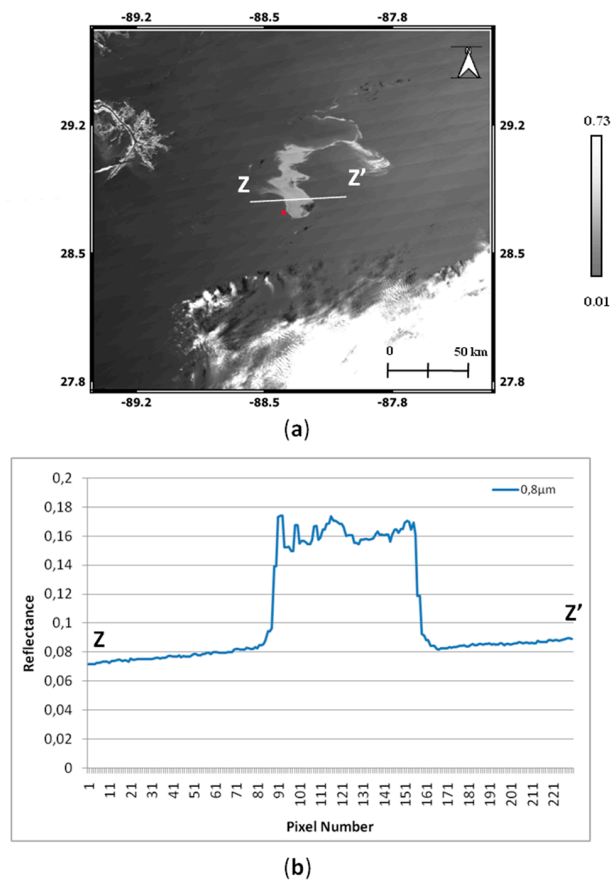


**Figure 5.** (a) MODIS Aqua image of 25 April 2010 at 18:55 GMT at 0.8  $\mu\text{m}$ . The red point indicates the DWH platform position. (b) Reflectance trend along the transect Z-Z'.

Results achieved by implementing the ALICE index (Equation (1)) on the MODIS 0.8  $\mu\text{m}$  channel ( $\otimes_{R0.8}$ ) for both previous images are shown in Figures 7 and 8, where land and clouds are masked in black and the red point indicates the DWH platform position.

Looking at the maps (Figures 7a and 8a), as well as at the ALICE profiles (Figures 7b and 8b) along the same transects of Figures 5 and 6, several considerations can be made. The first evident result is that, in both images, the entire scene shows values that are statistically significant, according to the RST approach (at least  $\otimes_{R0.8} > 2$ ), which also becomes very high ( $\otimes_{R0.8} > 8$ ) over a large area. This means that the whole scene is apparently in an anomalous condition, i.e., the reflectance recorded for almost all of the sea surfaces is higher than expected, which does not make any clear detection of the oil presence and position possible.

Focusing on the platform area and analyzing ALICE profiles along the two transects (Z-Z' and T-T'), a clear increase is visible for both images. In detail,  $\otimes_{R0.8}$  reaches values of up to 50 in the oil affected area, likely as a consequence of the higher NIR signal absorption by water, which emphasizes contrast between reflecting bodies (e.g., oil) and the surrounding water. Despite this behavior, such a signal increase cannot be easily isolated in the whole scene without implementing other further processing steps (i.e., image segmentation, image classification, spatial filter, and ROI extraction), which may reduce the accuracy of a fully automatic detection system as well as increasing its elaboration time, especially if the presence of an operator is required.

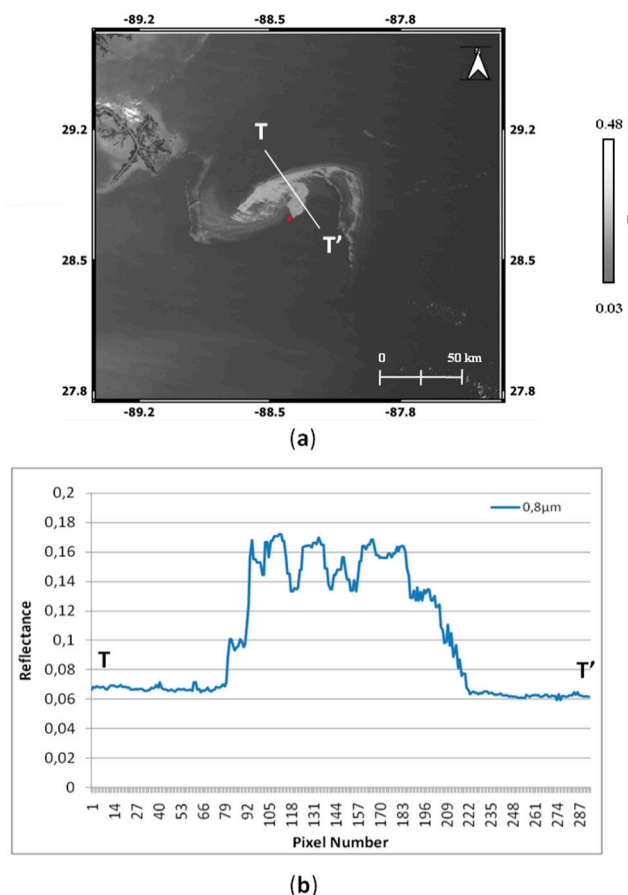


**Figure 6.** (a) MODIS Terra image of 29 April 2010 at 16:55 GMT at 0.8  $\mu\text{m}$ . The red point indicates the DWH platform position. (b) Reflectance trend along the transect T-T'.

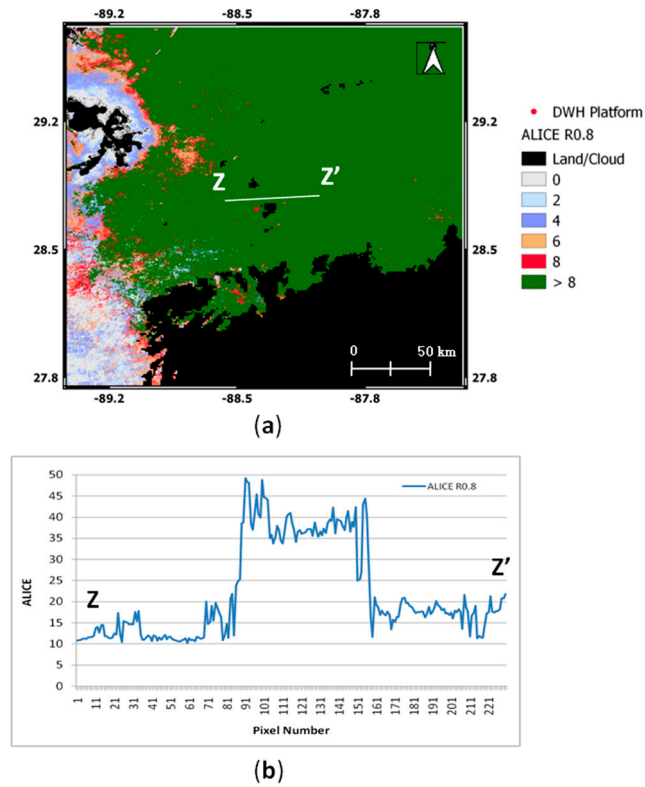


Figure 7. (a) ALICE ( $\otimes_{R0.8}$ ) map relative to the MODIS image shown in Figure 4a and (b) relative trend along the transect.

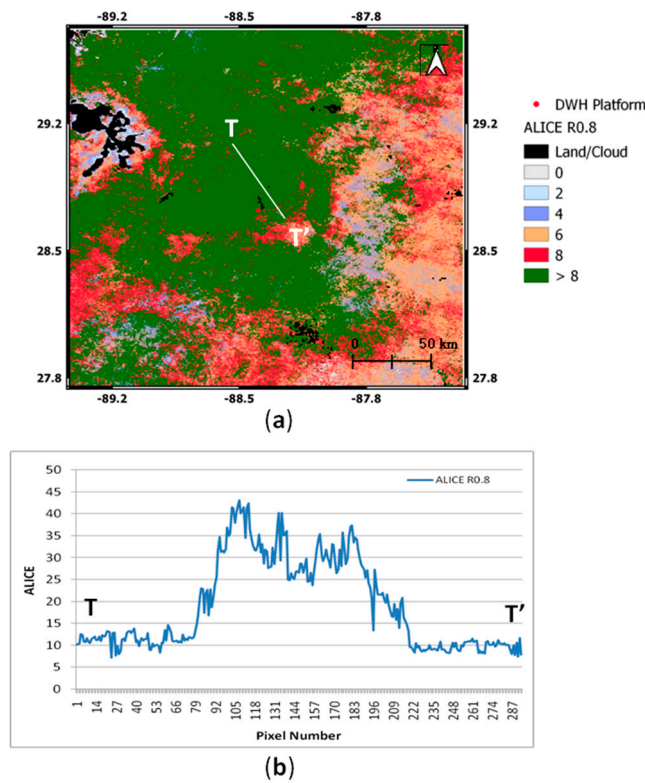
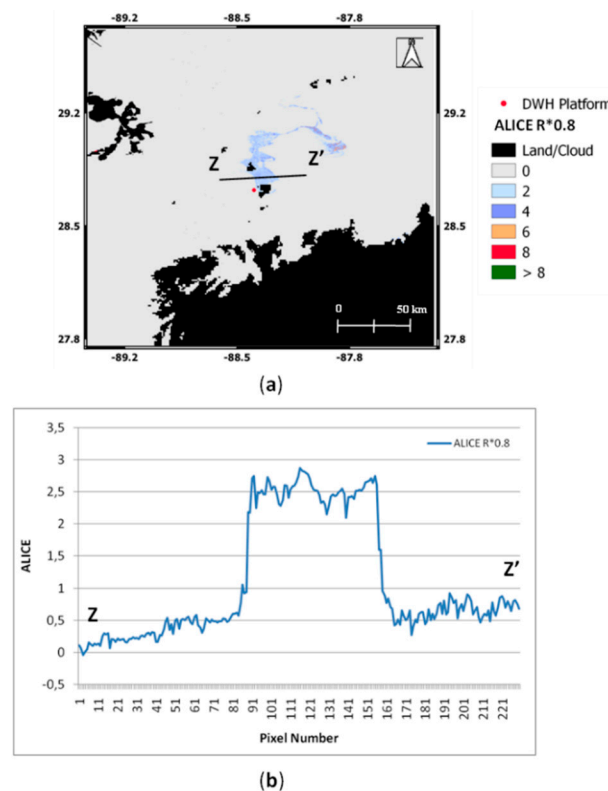


Figure 8. The same as in Figure 7 for the MODIS Terra image of Figure 4b.

### 3.2. Results of the Advanced RST-OIL Configuration

According to the advanced RST-OIL configuration proposed in this study (Section 2.3, Equation (2)), we found that the Aqua image (Figure 4a) was completely acquired under high glint conditions while the Terra one (Figure 4b) showed dual behavior with a zone affected by high glint (top left) and the remaining portion was under glint conditions. The new proposed approach (Equation (3)) was implemented on both previously analyzed images (Figures 7 and 8). The results are shown in Figures 9 and 10.



**Figure 9.** (a)  $ALICE_{R^{*0.8}}$  ( $\otimes_{R^{*0.8}}$ ) map relative to the MODIS Aqua image of Figure 4a and (b) the relative trend along the transect.

The improvements of the proposed configuration in terms of reliability are evident. In both images, the  $\otimes_{R^{*0.8}}$  values measured in not oil-contaminated areas are always below 2 sigma, which indicates their acquisition in “normal” conditions (i.e., homogeneous with those represented by the reference fields). The comparison between an image acquired under glint (or high glint) conditions and the corresponding reference fields enables discrimination between the (absolute) high reflectance values due to sun-satellite geometry and the (relative) increase only ascribable to the oil presence.

Results obtained by implementing the new RST-OIL configuration on all the MODIS images available during the considered period (April–May 2010) and acquired under sun glint conditions are shown in Figure 11 together with the corresponding RGB imagery. In all figures, the oil-affected areas are identified and very well isolated with respect to the clean seawater areas. Values of anomalous areas are always statistically significant (ranging from  $\sim 2$  to  $\sim 8$ ) and consistent when moving from one image to another, which allows for automatic and unsupervised identification as well as effective monitoring of the evolution, in terms of the intensity and extent of the spilled areas. Moreover, false positives do not seem to significantly affect the scenes analyzed in this case, which confirms the good reliability of the improved method, even under these severe sun glint conditions. On the other hand, some limits appear evident: (i) the cloud coverage is likely over-estimated and (ii) the sensitivity of the method is sometimes lower than expected. Regarding the cloud mask, it is worth mentioning that, in this work, only the TIR channel has been used to implement the OCA approach (Section 2.2), where

it is generally applied by combining TIR and VIS information to obtain more accurate results (some clouds may, in fact, show signatures only in one spectral region). Unfortunately, in the VIS region, clouds and oil often exhibit similar spectral behavior and, therefore, it was not possible to use the VIS band in this scenario to discriminate among clouds. Therefore, the obtained cloud mask may suffer from a lack of accuracy. Concerning the RST-OIL sensitivity, the underestimation of oil slicks coming from a visual comparison between  $ALICE_{R*0.8}$  maps and corresponding RGB imagery may be a direct consequence of the previously mentioned cloud mask inaccuracy, since the spilled areas might be simply covered by the (supposed) cloudy radiances. In addition, the oil status, type, and thickness may further affect the spectral behavior and, consequently, the RST-OIL capability in correctly detecting spilled zones. However, it should be stressed in this study that the main aim of the algorithm is not providing a detailed mapping of the spill but promptly detecting the possible oil presence on the scene in order to give a timely alert. In this sense, even a single oil pixel detection represents a good result.

In the results shown above, we focused only on oil characterized by a positive contrast compared with surrounding waters. As discussed in Section 3.1, such a condition represents a critical situation for the standard RST configuration. In any case, as already mentioned in Section 1, oil can exhibit a negative contrast, even under sun glint conditions. To test the behavior of the proposed index (Equation (3)), in this second case, we also analyzed the Aqua image from 27 May 2010 at 18:55 (Figure 12a, totally acquired under high glint conditions) in which the oil appears in both positive (offshore area, NE corner) and negative (near shoreline, SW corner) contrast. Figure 12b shows the corresponding  $\otimes_{R*0.8}$  index output: almost all of the area covered by oil in a positive contrast (violet area) has been detected, which is in line with the results already presented in Figures 9–11. Regarding the negative contrast zone, it has also been detected with negative  $\otimes_{R*0.8}$  values lower than  $-1$  (yellow pixels). As already mentioned, this is an expected output, considering the very low NIR signal (close to 0) of water for unperturbed conditions, which reduces the  $\otimes_{R*0.8}$  dynamic range.

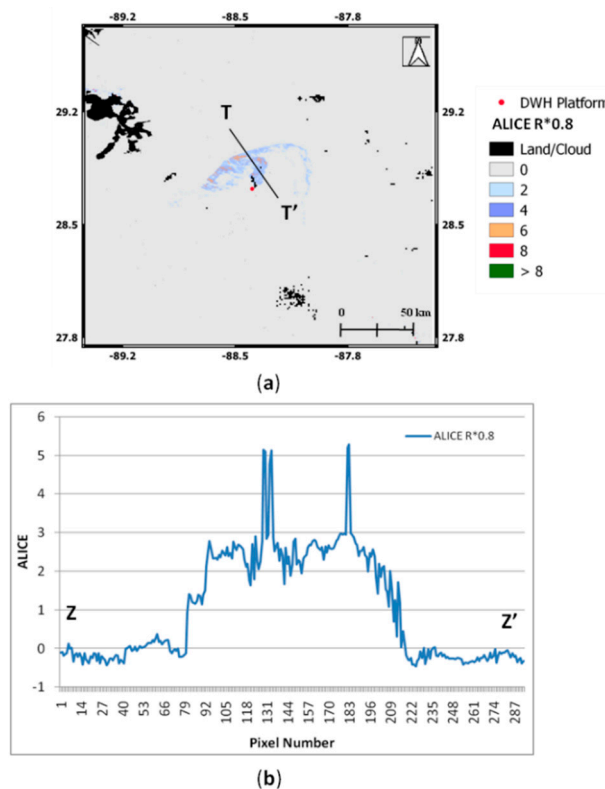


Figure 10. The same as in Figure 8 for the MODIS Terra image of Figure 4b.

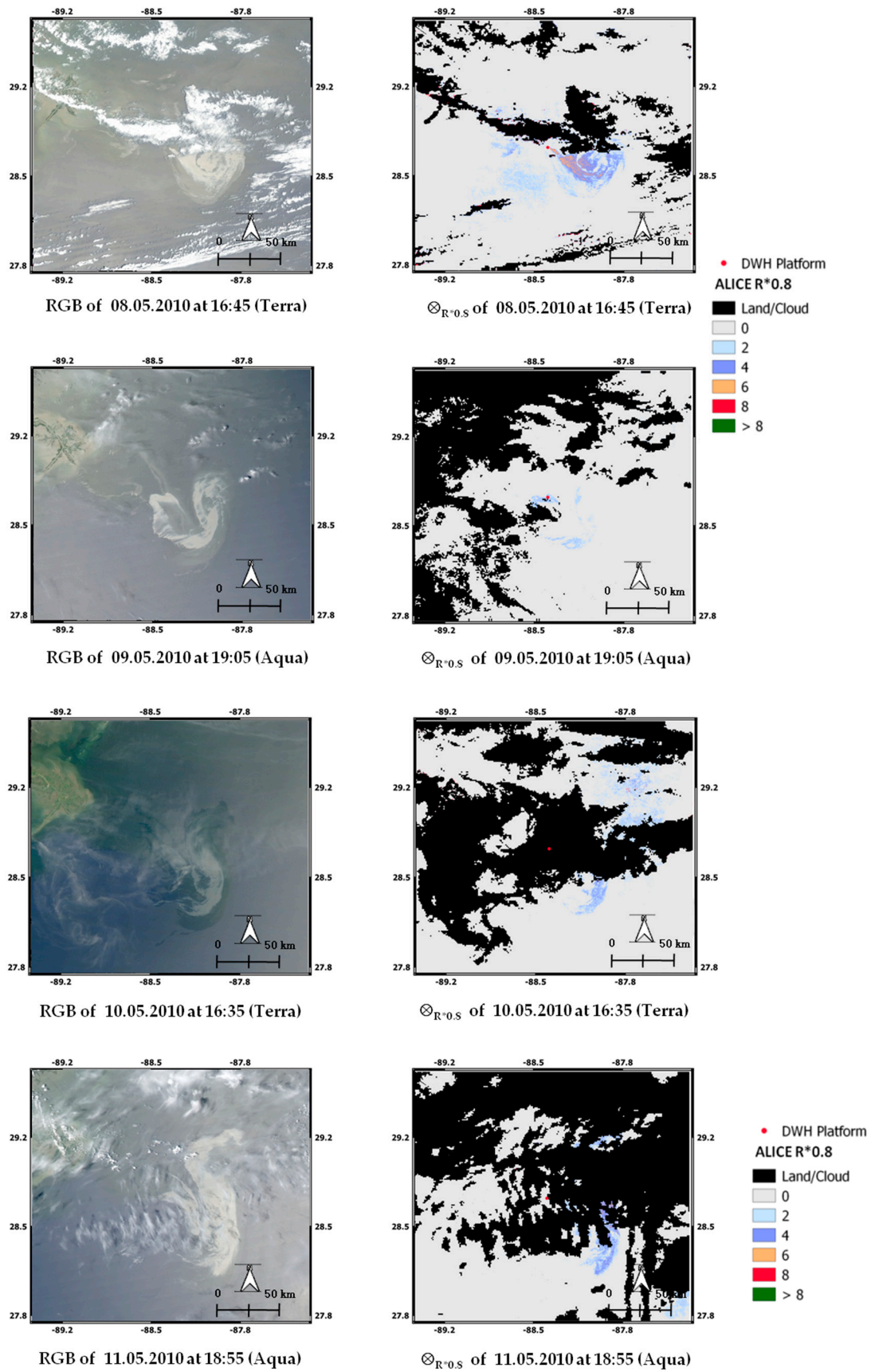
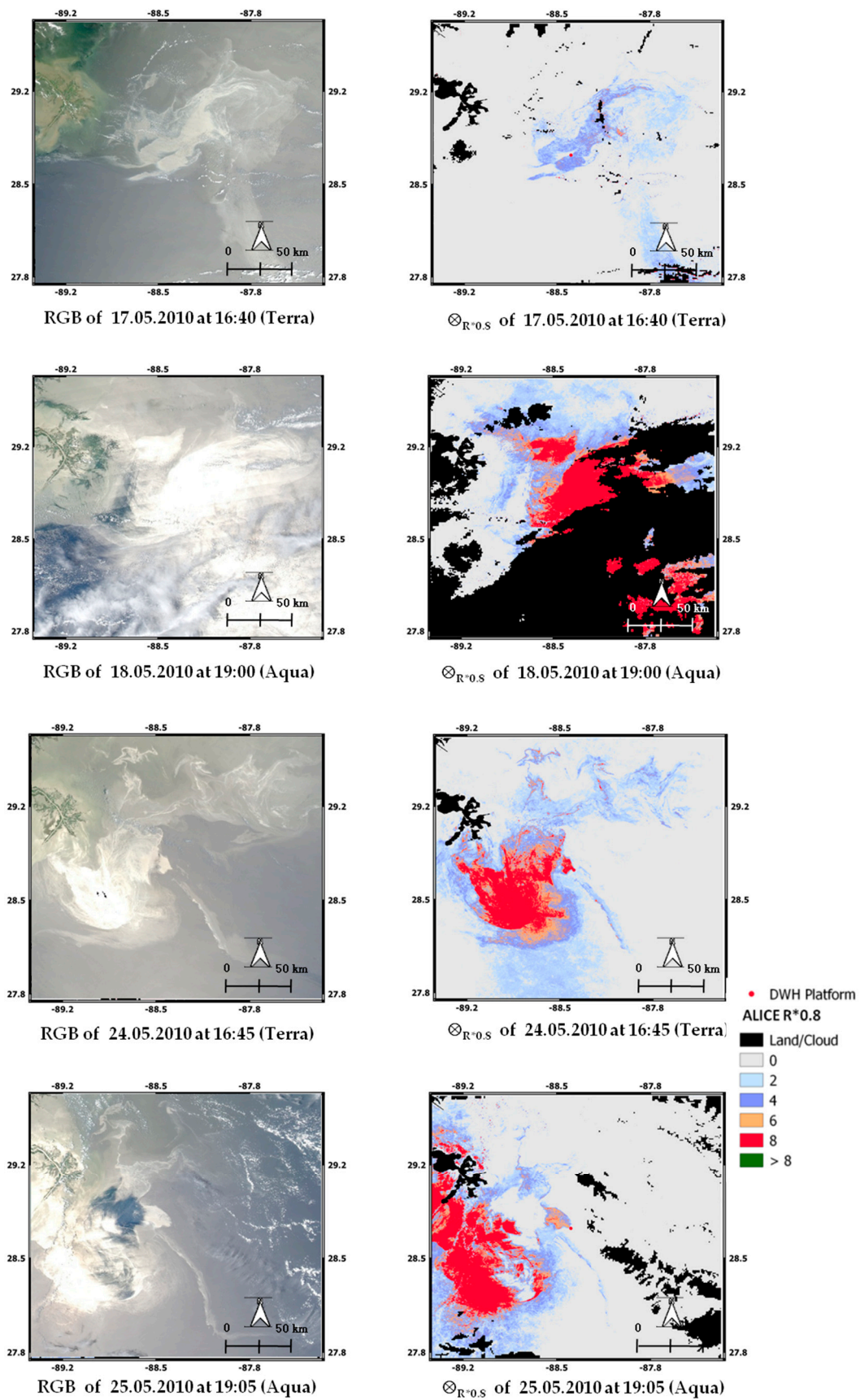
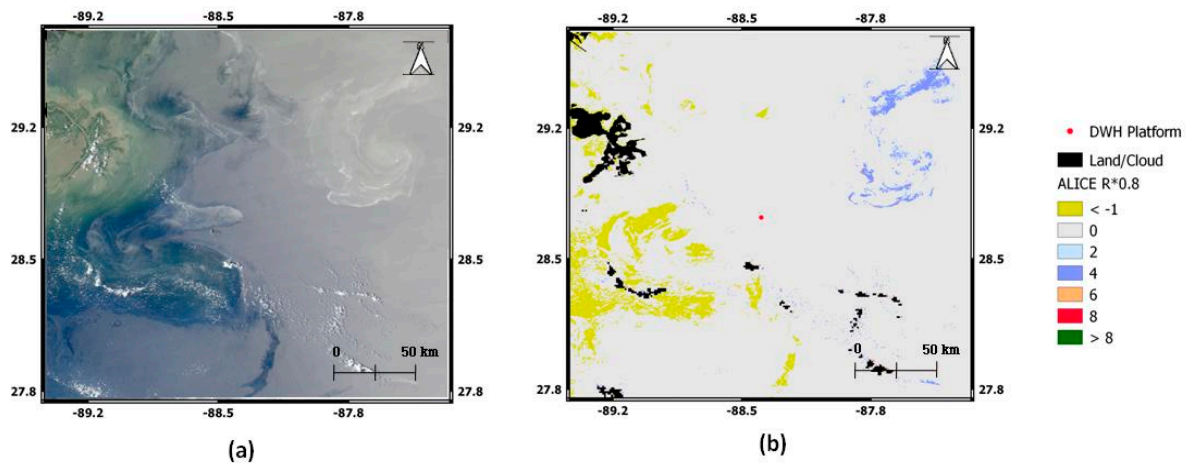


Figure 11. Cont.



**Figure 11.** New approach results for all images available in the period April–May 2010 together with the corresponding true-color RGB.



**Figure 12.** (a) RGB of the MODIS Aqua image from 27 May 2010 at 18:55, (b)  $ALICE_{R^*0.8}$  ( $\otimes_{R^*0.8}$ ) map relative to the same image.

Such a behavior is clearly observed in Figure 13, showing the 0.8  $\mu\text{m}$  reflectance variability (red line) along the Y-Y' transect shown in Figure 13a. In the graph, the temporal mean (black line) along the segment as well as the  $\pm 1$  interval range of variability (gray lines) have been plotted.

Looking at the figure, the oil affected areas (at the beginning and the end of the red line) are clearly characterized by “anomalous” reflectance with respect to the expected (i.e., mean) value, even considering its normal fluctuation (i.e.,  $\pm 1$  sigma). However, in case of a positive contrast, the reflectance may increase significantly, and, when negative contrast occurs, observed values decrease but do not move much lower from the expected signal. Since the reflectance is limited to positive values, it cannot allow for higher negative  $\otimes_{R^*0.8}$  values, which results, in some cases, in sensitivity issues or missing detections (i.e., false negatives). This is what has been observed for the Terra image acquired on 10 May 2010 at 16:35 (Figure 11) where the proposed approach was not able to detect any spill and showed a negative contrast.

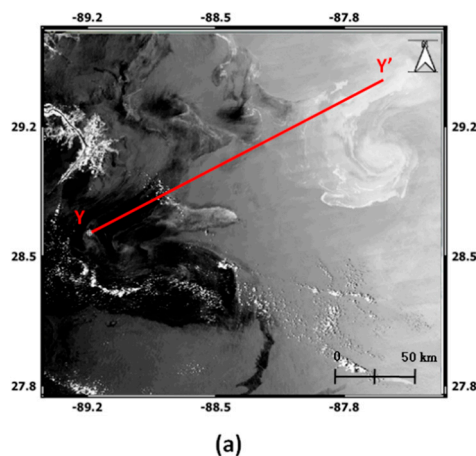
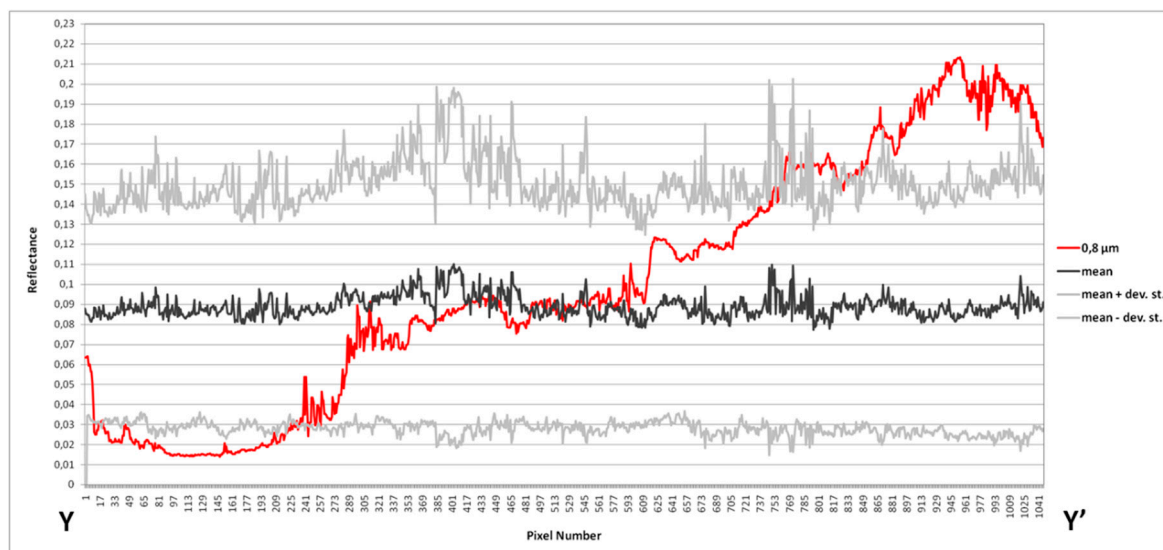


**Figure 13.** Cont.



(b)

**Figure 13.** (a) MODIS Aqua image from 27 May 2010 at 18:55 at 0.8  $\mu\text{m}$ . (b) Reflectance trend along the Y-Y' transect compared with mean and mean  $\pm$  sigma trends.

#### 4. Discussion

In the framework of oil spill detection by satellite techniques based on VNIR data, the occurrence of sun glint conditions can be seen as an added value that is helpful for the discrimination between oil slicks and the surrounding water for almost all the techniques developed so far [5,15,17,23,46–48]. Techniques that work in such conditions strongly depend on the use of ancillary data (e.g., wind speed, aerosol characterization), which are often site-related and not always available, which limits their accuracy as well as their exportability. On the other hand, as widely explained in Section 2.3, the previously mentioned added value is not a favorable element for multi-temporal techniques based on historical signal variation analysis. Therefore, a methodology, like the one presented in this case, which is able to automatically manage images acquired under peculiar observation conditions by exploiting only satellite data, can guarantee a clear advantage, especially for operational and real-time applications. The unavailability of all the information/data necessary for implementing other optical techniques prevented a direct assessment of the results achieved in this work. Therefore, the results presented in this paper were assessed by comparing with the outputs obtained independently by another methodology based on active microwave data. The Textural Classifier Neural Network Algorithm (TCNNA) methodology [44] was developed for SAR-Envisat data to map the spill resulting from DWH platform explosion. The algorithm simultaneously processes SAR images and ancillary wind data (obtained as outputs from the geophysical model CMOD5) [44,49] by using a combination of two Neural Networks (NN). The first NN identifies pixels potentially affected by oil when they become the input to the second NN, which performs a statistical textural analysis to definitively discriminate floating oil [19]. The final product is a map of the affected spill area, which can be downloaded as a shape file from the Environmental Response Management Application (ERMA) web application [50].

SAR data used by the TCNNA methodology have different acquisition times compared to MODIS scenes used in this study. To assess our results, two shape files were downloaded from the ERMA website: one relative to the TCNNA result produced by analyzing the TerraSAR image from 25 April 2010 at 11:50 GMT (acquired about 7 h earlier than the MODIS Aqua one) and another one generated using the Envisat data from 29 April 2010 at 03:45 GMT (acquired 13 h earlier than the MODIS Terra one) (Figure 14).

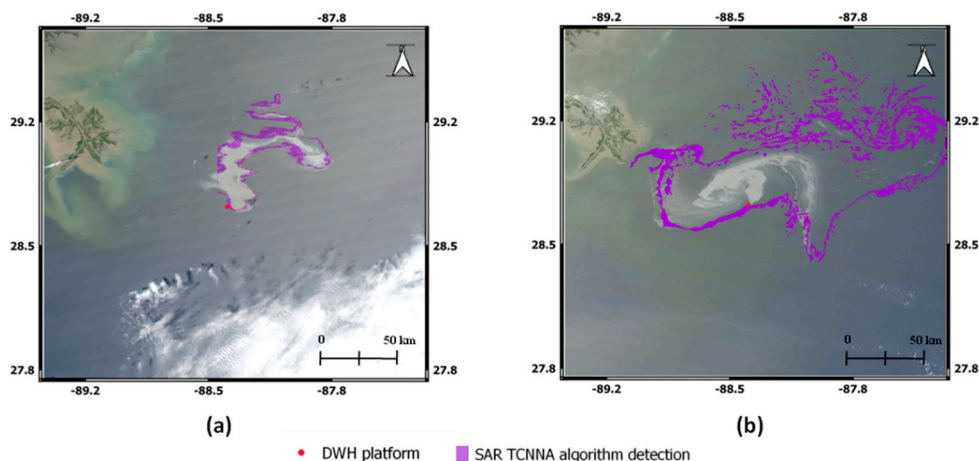


**Figure 14.** TCNNA shape files (violet) for (a) 25 April 2010 at 11:50 GMT (TerraSAR) data (overlapping on MODIS RGB of 25 April 2010 at 18:55 GMT) and (b) 29 April 2010 at 03:45 GMT (Envisat) data (overlapping on MODIS RGB of 29 April 2010 at 16:55).

The comparison between the two methodologies is shown in Figure 15 where pixels detected by the new RST-OIL approach possibly affected by oil are highlighted in green (considering  $\otimes_{R^{*0.8}} > 2$ ), whereas the TCNNA spilled areas are depicted in violet. The overlapping of the two maps shows that ~99% of the pixels detected by the methodology proposed in this work are within the oil-affected areas and are identified by TCNNA, which confirms the high reliability of RST-OIL for effectively detecting the presence of an oil spill.

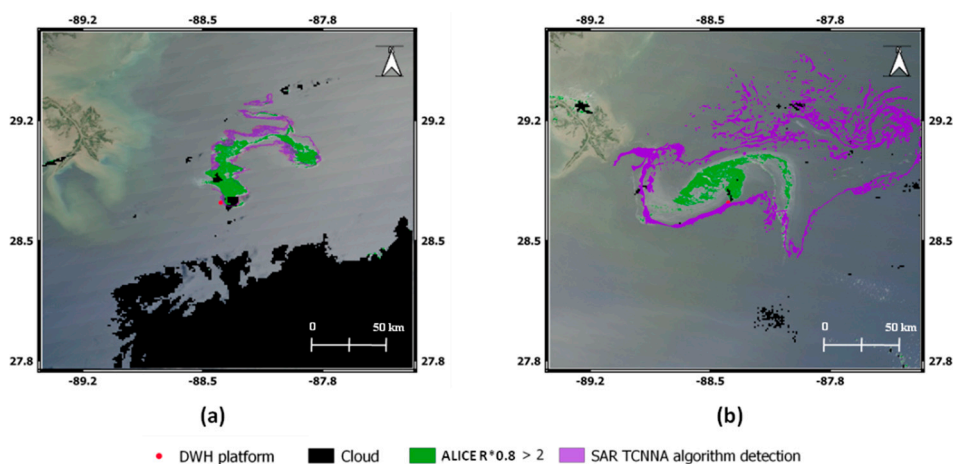


**Figure 15.** Comparison between the new proposed RST-OIL approach (green) and the TCNNA methodology (violet) for both test case images: (a) 25 April 2010 at 18:55, and (b) 29 April 2010 at 16:55.

Focusing on Figure 15a, in which the temporal gap between the two images is lower and the matching is more accurate, we found that TCNNA detected about 1100 km<sup>2</sup> of oil (area within violet line), of which RST-OIL identified about 700 km<sup>2</sup> (green pixels), which left about 36% of the oil area undetected. The difference in terms of detected area extension may have been due to some factors, such as (i) the different spatial resolution between the data used, with values of about 20 m and 150 m for TerraSAR and SAR-Envisat, respectively, against the 250 m relative to the MODIS sensor, and (ii) the time gap between microwave and optical data acquisition time (7 h for TerraSAR and 13 h for Envisat, respectively). Regardless, the results obtained are still satisfactory because it is worth mentioning that the main goal of the technique proposed is not to provide detailed oil mapping but to give an effective and timely alert in case of an accident.

Through the analyzed MODIS time-series images (Figures 9–11), it was possible to estimate the accidental oil evolution in the temporal domain (Figure 16).

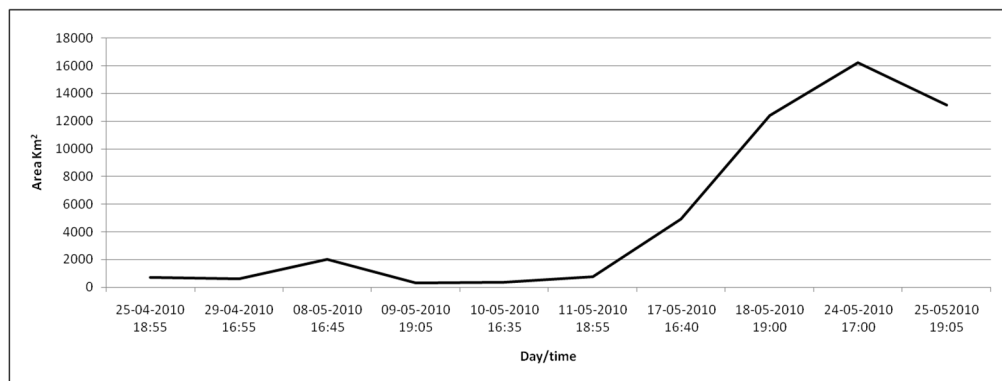


**Figure 16.** Oil area (km<sup>2</sup>) temporal trend for the period analyzed.

Despite the possible oil slick underestimation discussed previously, the oil area profile reported in Figure 16 is in very good agreement with the results of another independent study [20], which coherently matches the phases that characterized the accident. The observed variability seems to be linked to a progressive oil accumulation. Once sunk, the DWH platform continued to spill oil into the sea, which accumulated more and more on the surface. Starting from 21 April 2010 (the day after the event), the competent authorities tried various actions to stop the oil spill [51]. In the first few days after the event, an attempt was made to act on the exhaust blocking valves. Then, an attempt was made to contain the spilled oil, and toward the end of May, the first operations to pump mud into the wells were attempted to try to cement it. However, all of these operations had no success. It is, therefore, necessary to wait for the month of June to witness the first successful interventions, which will be completed at the end of July with the entire containment of the spill.

The results achieved in this work indicate a few limitations of the proposed approach. Cloud cover affects the achieved results with a two-fold contribution. On one hand, clouds may completely mask the sea surface, hampering any detection. On the other hand, a cloud mask that is not completely accurate may affect the accuracy of the produced outputs. Few areas could not be considered in the analysis because they were erroneously detected as being affected by the cloud. Further analyses have to be carried out on this topic to refine cloud detection schemes and further enhance the quality of the achieved results. Moreover, oil slick characterized by a negative contrast may be difficult to discriminate from the surrounding waters due to the very low range of variability of the investigated signal under such conditions, which is also very complicated for detection from a statistical point of view. A possible solution to face such an issue could be to consider, as an unperturbed condition, the minimum historically recorded value at the pixel level in place of the medium one.

Proposed work can be open to other future developments, which may even involve exploiting the advanced capabilities offered by new generation sensors, such as the Ocean and Land Color Instrument (OLCI) onboard the Copernicus Sentinel-3 mission (in orbit since April 2018). The instrument, which has a similar spatial resolution to MODIS (i.e., 300 m), has a higher spectral capability and was specifically developed for sea surface observation. Furthermore, OLCI data may be integrated with those acquired by the Multi Spectral Imager (MSI) onboard the Copernicus Sentinel-2. This sensor, which is fully operational on both Sentinel-2A (in orbit since June 2015) and Sentinel-2B (in orbit since March 2017) ensures the availability of data with a spatial resolution of up to 10 m in the VNIR bands, which allows an increase in sensitivity, even for small spills.

## 5. Conclusions

In this paper, an innovative configuration of RST-OIL was applied to MODIS NIR data at a spatial resolution of 250 m. In particular, this configuration was developed to detect the presence of oil under

extreme observation conditions occurring, for example, in the presence of a (high/moderate) sun glint effect. The obtained results were satisfactory with a reliability of up to 99% when compared with those achieved by a SAR-based methodology. A sensitivity accuracy of about 60% was also found, which, considering that a detailed mapping of the oil-affected areas was outside the scope of this paper, can be considered acceptable. Oil-affected areas, in positive contrast with surrounding seawater, were detected without any false alarm and with a good signal-to-noise ratio. Concerning oil in a negative contrast, although some limits related to the technique configuration exist, the oil area was detected even with a signal-to-noise ratio slightly lower than the previous case.

It is worth explaining that, even though these results came out of a single case study (DeepWater Horizon accident), the numerous images available (acquired at different date-times and by different satellites) allow the analyses to be performed under boundary conditions (observation, environmental, and atmospheric), which are so different from each other that they could be considered independent.

Considering the results already achieved by the same method using TIR data, RST-OIL can be seen as a suitable operational tool for the automatic and timely detection of oil spills, which is critical as a rapid response to oil spills using numerical models [52]. This is possible without any other ancillary/auxiliary data, which makes the techniques fully automatic and easily exportable everywhere. Furthermore, RST-OIL can be integrated with outputs coming from the SAR data analysis to improve the spatial resolution and provide an all-day/weather capability. Additionally, RST-OIL can be used jointly with other independent techniques that are better suited to mapping spilled areas in order to build a more effective satellite-based oil spill monitoring system.

**Author Contributions:** Conceptualization, V.S. and T.L.; Data curation, V.S. and E.C.; Formal analysis, V.S.; Investigation, V.S. and T.L.; Methodology, N.P. and V.T.; Software, V.S.; Supervision, T.L.; Validation, V.S.; Writing—original draft, V.S. and T.L.; Writing—review & editing, E.C., T.L., N.P. and V.T.

**Funding:** SAPERE (Space Advanced Project Excellence in Research and Enterprise) project financed by MIUR, CTN01\_00236, partly funded this research.

**Conflicts of Interest:** The authors declare no conflict of interest.

## References

1. Global Marine Oil Pollution Information Gateway Web Site. Available online: <http://oils.gpa.unep.org/facts/sources.htm> (accessed on 9 September 2019).
2. National Research Council. *Oil in the Sea III: Inputs, Fates, and Effects*; The National Academies Press: Washington, DC, USA, 2003.
3. ITOPF Web Site. Available online: <http://www.itopf.com/knowledge-resources/data-statistics/statistics/> (accessed on 9 September 2019).
4. Ribotti, A.; Antognarelli, F.; Cucco, A.; Falcieri, M.; Fazioli, L.; Ferrarin, C.; Satta, A. An Operational Marine Oil Spill Forecasting Tool for the Management of Emergencies in the Italian Seas. *J. Mar. Sci. Eng.* **2019**, *7*, 1. [[CrossRef](#)]
5. Fingas, M.; Brown, C.E. A Review of Oil Spill Remote Sensing. *Sensors* **2017**, *18*, 91. [[CrossRef](#)] [[PubMed](#)]
6. Pavlakis, P.; Sieber, A.; Alexandry, S. Monitoring oil-spill pollution in the Mediterranean with ERS SAR. *Oceanogr. Lit. Rev.* **1997**, *9*, 1067.
7. Fiscella, B.; Giancaspro, A.; Nirchio, F.; Pavese, P.; Trivero, P. Oil spill detection using marine SAR images. *Int. J. Remote Sens.* **2000**, *21*, 3561–3566. [[CrossRef](#)]
8. De Miranda, F.P.; Marmol, A.M.Q.; Pedroso, E.C.; Beisl, C.H.; Welgan, P.; Morales, L.M. Analysis of RADARSAT-1 data for offshore monitoring activities in the Cantarell Complex, Gulf of Mexico, using the unsupervised semivariogram textural classifier (USTC). *Can. J. Remote Sens.* **2004**, *30*, 424–436. [[CrossRef](#)]
9. Brekke, C.; Solberg, A.H.S. Review on Oil spill detection by satellite remote sensing. *Remote Sens. Environ.* **2005**, *95*, 1–13. [[CrossRef](#)]
10. Ferraro, G.; Bernardini, A.; David, M.; Meyer-Roux, S.; Muellenhoff, O.; Perkovic, M.; Tarchi, D.; Topouzelis, K.; Topouzelis, K. Towards an operational use of space imagery for oil pollution monitoring in the Mediterranean basin: A demonstration in the Adriatic Sea. *Mar. Pollut. Bull.* **2007**, *54*, 403–422. [[CrossRef](#)]

11. Akkartal, A.; Sunar, F. The usage of RADAR images in oil spill detection. *Int. Arch. Photogramm. Remote Sens. Spat. Inf. Sci.* **2008**, *37*, 8.
12. Marghany, M. Utilization of a genetic algorithm for the automatic detection of oil spill from RADARSAT-2 SAR satellite data. *Mar. Pollut. Bull.* **2014**, *89*, 20–29. [[CrossRef](#)]
13. Agenzia Spaziale Italiana. System Description & User Guide. COSMO-SkyMed. Available online: <http://www.cosmo-skymed.it/docs/ASI-CSM-ENG-RS-093-A-CSKSysDescriptionAndUserGuide.pdf> (accessed on 9 September 2019).
14. Cross, A. Monitoring marine oil pollution using AVHRR data: Observations off the coast of Kuwait and Saudi Arabia during January 1991. *Int. J. Remote Sens.* **1992**, *13*, 781–788. [[CrossRef](#)]
15. Hu, C.; Müller-Karger, F.E.; Taylor, C.; Myhre, D.; Murch, B.; Odriozola, A.L.; Godoy, G.; Muller-Karger, F.E. MODIS detects oil spills in Lake Maracaibo, Venezuela. *Eos Trans. Am. Geophys. Union* **2003**, *84*, 313. [[CrossRef](#)]
16. Howari, F.M. Investigation of Hydrocarbon Pollution in the Vicinity of United Arab Emirates Coasts Using Visible and Near Infrared Remote Sensing Data. *J. Coast. Res.* **2004**, *204*, 1089–1095. [[CrossRef](#)]
17. Shi, L.; Zhang, X.; Seielstad, G.; Zhao, C.; He, M.-X.; Shi, L. Oil Spill Detection by MODIS Images using Fuzzy Cluster and Texture Feature Extraction. In Proceedings of the OCEANS 2007—Europe, Aberdeen, UK, 18–21 June 2007; pp. 1–5.
18. Dessì, F.; Melis, M.T.; Naitza, L.; Marini, A. MODIS data processing for coastal and marine environment monitoring: A study on anomaly detection and evolution in gulf of Cagliari (Sardinia-Italy). *Int. Arch. Photogramm. Remote Sens. Spat. Inf. Sci.* **2008**, *37-B8*, 695–698.
19. Etellisi, E.A.; Deng, Y. Oil spill detection: Imaging system modeling and advanced image processing using optimized SDC algorithm. *Signal Image Video Process.* **2014**, *8*, 1405–1419. [[CrossRef](#)]
20. Maianti, P.; Rusmini, M.; Tortini, R.; Via, G.D.; Frassy, F.; Marchesi, A.; Nodari, F.R.; Gianinetto, M. Monitoring large oil slick dynamics with moderate resolution multispectral satellite data. *Nat. Hazards* **2014**, *73*, 473–492. [[CrossRef](#)]
21. Zhao, J.; Temimi, M.; Ghedira, H.; Hu, C. Exploring the potential of optical remote sensing for oil spill detection in shallow coastal waters—A case study in the Arabian Gulf. *Opt. Express* **2014**, *22*, 13755–13772. [[CrossRef](#)]
22. Laneve, G.; Luciani, R. Developing a satellite optical sensor based automatic system for detecting and monitoring oil spills. In Proceedings of the 2015 IEEE 15th International Conference on Environment and Electrical Engineering (EEEIC), Rome, Italy, 10–13 June 2015; pp. 1653–1658.
23. Pisano, A.; Bignami, F.; Santoleri, R. Oil Spill Detection in Glint-Contaminated Near-Infrared MODIS Imagery. *Remote Sens.* **2015**, *7*, 1112–1134. [[CrossRef](#)]
24. Zhao, J.; Temimi, M.; Al Azhar, M.; Ghedira, H. Satellite-Based Tracking of Oil Pollution in the Arabian Gulf and the Sea of Oman. *Can. J. Remote Sens.* **2015**, *41*, 113–125. [[CrossRef](#)]
25. Asanuma, I.; Muneyama, K.; Sasaki, Y.; Iisaka, J.; Yasuda, Y.; Emori, Y. Satellite thermal observation of oil slicks on the persian gulf. *Remote Sens. Environ.* **1986**, *19*, 171–186. [[CrossRef](#)]
26. Borzelli, G.; Ciappa, A.; Ulivieri, C.; Antonelli, G.; Laneve, G. A new perspective on oil slick detection from space by NOAA satellites. *Int. J. Remote Sens.* **1996**, *17*, 1279–1292. [[CrossRef](#)]
27. Casciello, D.; Lacava, T.; Pergola, N.; Tramutoli, V. Robust Satellite Techniques (RST) for oil spill detection and monitoring using AVHRR Thermal Infrared bands. *Int. J. Remote Sens.* **2011**, *32*, 4107–4129. [[CrossRef](#)]
28. Grimaldi, C.S.L.; Coviello, I.; Lacava, T.; Pergola, N.; Tramutoli, V.; Liu, Y.; MacFadyen, A.; Ji, Z.-G.; Weisberg, R.H. A New RST-Based Approach for Continuous Oil Spill Detection in TIR Range: The Case of the Deepwater Horizon Platform in the Gulf of Mexico. In *Monitoring and Modeling the Deepwater Horizon Oil Spill: A Record-Breaking Enterprise*; American Geophysical Union (AGU): Washington, DC, USA, 2011; Volume 195, pp. 19–31.
29. Salisbury, J.W.; D’Aria, D.M.; Sabins, F.F. Thermal infrared remote sensing of crude oil slicks. *Remote Sens. Environ.* **1993**, *45*, 225–231. [[CrossRef](#)]
30. Jha, M.N.; Levy, J.; Gao, Y. Advances in Remote Sensing for Oil Spill Disaster Management: State-of-the-Art Sensors Technology for Oil Spill Surveillance. *Sensors* **2008**, *8*, 236–255. [[CrossRef](#)] [[PubMed](#)]
31. Otremba, Z.; Piskozub, J. Modelling of the optical contrast of an oil film on a sea surface. *Opt. Express* **2001**, *9*, 411–416. [[CrossRef](#)]

32. Otremba, Z.; Piskozub, J. Modeling the remotely sensed optical contrast caused by oil suspended in the sea water column. *Opt. Express* **2003**, *11*, 2–6. [[CrossRef](#)]
33. Haule, K.; Freda, W.; Darecki, M.; Toczek, H. Possibilities of optical remote sensing of dispersed oil in coastal waters. *Estuar. Coast. Shelf Sci.* **2017**, *195*, 76–87. [[CrossRef](#)]
34. Otremba, Z. Oil Droplet Clouds Suspended in the Sea: Can They Be Remotely Detected? *Remote Sens.* **2016**, *8*, 857. [[CrossRef](#)]
35. Tramutoli, V. Robust AVHRR techniques (RAT) for environmental monitoring: Theory and applications. *Remote Sens.* **1998**, *3496*, 101–113.
36. Casciello, D.; Grimaldi, C.S.L.; Coviello, I.; Lacava, T.; Pergola, N.; Tramutoli, V. A Robust Satellite Techniques for oil spill detection and monitoring in the optical range. In *Global Monitoring for Security and Stability (GMOSS), JRC Scientific and Technical Reports*; EUR 23033 EN; Zeug, G., Pesaresi, M., Eds.; OPOCE: Luxembourg, 2007; pp. 294–305. [[CrossRef](#)]
37. Grimaldi, C.S.L.; Casciello, D.; Coviello, I.; Lacava, T.; Pergola, N.; Tramutoli, V. An improved RST approach for timely alert and Near Real Time monitoring of oil spill disasters by using AVHRR data. *Nat. Hazards Earth Syst. Sci.* **2011**, *11*, 1281–1291. [[CrossRef](#)]
38. Lacava, T.; Ciancia, E.; Coviello, I.; Di Polito, C.; Grimaldi, C.S.L.; Pergola, N.; Satriano, V.; Temimi, M.; Zhao, J.; Tramutoli, V. A MODIS-Based Robust Satellite Technique (RST) for Timely Detection of Oil Spilled Areas. *Remote Sens.* **2017**, *9*, 128. [[CrossRef](#)]
39. Liu, Y.; MacFadyen, A.; Ji, Z.-G.; Weisberg, R.H. (Eds.) *Monitoring and Modeling the Deepwater Horizon Oil Spill: A Record Breaking Enterprise*; Geophysical Monograph Series; AGU: Washington, DC, USA, 2011; Volume 195, p. 271.
40. NASA-LAADS DAAC Web. Available online: <https://ladsweb.modaps.eosdis.nasa.gov/search/> (accessed on 9 September 2019).
41. Di Polito, C.; Ciancia, E.; Coviello, I.; Doxaran, D.; Lacava, T.; Pergola, N.; Satriano, V.; Tramutoli, V. On the Potential of Robust Satellite Techniques Approach for SPM Monitoring in Coastal Waters: Implementation and Application over the Basilicata Ionian Coastal Waters Using MODIS-Aqua. *Remote Sens.* **2016**, *8*, 922. [[CrossRef](#)]
42. Cuomo, V.; Filizzola, C.; Pergola, N.; Pietrapertosa, C.; Tramutoli, V. A self-sufficient approach for GERB cloudy radiance detection. *Atmos. Res.* **2004**, *72*, 39–56. [[CrossRef](#)]
43. Jackson, C.R.; Alpers, W. The role of the critical angle in brightness reversals on sun glint images of the sea surface. *J. Geophys. Res. Ocean.* **2010**, *115*. [[CrossRef](#)]
44. Garcia-Pineda, O.; Macdonald, I.R.; Li, X.; Jackson, C.R.; Pichel, W.G. Oil Spill Mapping and Measurement in the Gulf of Mexico with Textural Classifier Neural Network Algorithm (TCNNA). *IEEE J. Sel. Top. Appl. Earth Obs. Remote Sens.* **2013**, *6*, 2517–2525. [[CrossRef](#)]
45. Hu, C.; Feng, L.; Holmes, J.; Swayze, G.A.; Leifer, I.; Melton, C.; García, O.; Macdonald, I.; Hess, M.; Muller-Karger, F.; et al. Remote sensing estimation of surface oil volume during the 2010 Deepwater Horizon oil blowout in the Gulf of Mexico: Scaling up AVIRIS observations with MODIS measurements. *J. Appl. Remote Sens.* **2018**, *12*, 026008. [[CrossRef](#)]
46. Leifer, I.; Lehr, W.J.; Simecek-Beatty, D.; Bradley, E.; Clark, R.; Dennison, P.; Hu, Y.; Matheson, S.; Jones, C.E.; Holt, B.; et al. State of the art satellite and airborne marine oil spill remote sensing: Application to the BP Deepwater Horizon oil spill. *Remote Sens. Environ.* **2012**, *124*, 185–209. [[CrossRef](#)]
47. Adamo, M.; De Carolis, G.; De Pasquale, V.; Pasquariello, G. Oil Spill Surveillance and Tracking with Combined use of SAR and Modis Imagery: A Case Study. In *Proceedings of the 2006 IEEE International Symposium on Geoscience and Remote Sensing*, Denver, CO, USA, 31 July–4 August 2006; pp. 1327–1330.
48. Adamo, M.; De Carolis, G.; De Pasquale, V.; Pasquariello, G. Detection and tracking of oil slicks on sun-glittered visible and near infrared satellite imagery. *Int. J. Remote Sens.* **2009**, *30*, 6403–6427. [[CrossRef](#)]
49. Hersbach, H.; Stoffelen, A.; De Haan, S. An improved C-band scatterometer ocean geophysical model function: Cmodj. *Geophys. Res. Space Phys.* **2007**, *112*. [[CrossRef](#)]
50. ERMA Web Site. Available online: <https://erma.noaa.gov/gulfofmexico/erma.html#/layers=3+17945+491+36355+36354+5328+482+18223+32680+32093+32957+32679+32211&x=-89.50988&y=29.80677&z=8&panel=layer> (accessed on 9 September 2019).

51. Gulf Spill Restoration Incident Overview. 2016. Available online: [https://www.gulfspillrestoration.noaa.gov/sites/default/files/wp-content/uploads/Chapter-2\\_Incident-Overview\\_508.pdf](https://www.gulfspillrestoration.noaa.gov/sites/default/files/wp-content/uploads/Chapter-2_Incident-Overview_508.pdf) (accessed on 9 September 2019).
52. Liu, Y.; Weisberg, R.H.; Hu, C.; Zheng, L.; MacFadyen, A.; Ji, Z.-G. Trajectory Forecast as a Rapid Response to the Deepwater Horizon Oil Spill. In *Monitoring and Modeling the Deepwater Horizon Oil Spill: A Record-Breaking Enterprise*; American Geophysical Union (AGU): Washington, DC, USA, 2011; Volume 195, pp. 153–165.



© 2019 by the authors. Licensee MDPI, Basel, Switzerland. This article is an open access article distributed under the terms and conditions of the Creative Commons Attribution (CC BY) license (<http://creativecommons.org/licenses/by/4.0/>).